Featured in Physics

Extraterrestrial Axion Search with the Breakthrough Listen Galactic Center Survey

Joshua W. Foster,[1,*] Samuel J. Witte,[2,†] Matthew Lawson,[3,4] Tim Linden,[3] Vishal Gajjar,[5] Christoph Weniger,[2] and Benjamin R. Safdi[6,7,‡]

[1]Center for Theoretical Physics, Massachusetts Institute of Technology, Cambridge, Massachusetts 02139, USA
[2]GRAPPA Institute, Institute for Theoretical Physics Amsterdam and Delta Institute for Theoretical Physics, University of Amsterdam, Science Park 904, 1098 XH Amsterdam, Netherlands
[3]The Oskar Klein Centre for Cosmoparticle Physics, Department of Physics, Stockholm University, Alba Nova, 10691 Stockholm, Sweden
[4]Nordita, KTH Royal Institute of Technology and Stockholm University, Roslagstullsbacken 23, 10691 Stockholm, Sweden
[5]Department of Astronomy, University of California Berkeley, Berkeley California 94720, USA
[6]Berkeley Center for Theoretical Physics, University of California, Berkeley, California 94720, USA
[7]Theoretical Physics Group, Lawrence Berkeley National Laboratory, Berkeley, California 94720, USA

(Received 14 March 2022; revised 30 July 2022; accepted 28 October 2022; published 13 December 2022)

Axion dark matter (DM) may efficiently convert to photons in the magnetospheres of neutron stars (NSs), producing nearly monochromatic radio emission. This process is resonantly triggered when the plasma frequency induced by the underlying charge distribution approximately matches the axion mass. We search for evidence of this process using archival Green Bank Telescope data collected in a survey of the Galactic Center in the *C* band by the Breakthrough Listen project. While Breakthrough Listen aims to find signatures of extraterrestrial life in the radio band, we show that their high-frequency resolution spectral data of the Galactic Center region is ideal for searching for axion-photon transitions generated by the population of NSs in the inner pc of the Galaxy. We use data-driven models to capture the distributions and properties of NSs in the inner Galaxy and compute the expected radio flux from each NS using state-of-the-art ray tracing simulations. We find no evidence for axion DM and set leading constraints on the axion-photon coupling, excluding values down to the level $g_{a\gamma\gamma} \sim 10^{-11}$ GeV^{-1} for DM axions for masses between 15 and 35 μeV.

DOI: 10.1103/PhysRevLett.129.251102

The quantum chromodynamics (QCD) axion is among the most well-motivated candidates for physics beyond the standard model, as it is capable of both resolving the strong *CP* problem and accounting for the observed dark matter (DM) abundance [1–7]. Axion masses spanning from $10 - 100$ μeV constitute a particularly compelling range of parameter space, as the DM abundance is arguably achieved most naturally for these candidates [8–14].

Recent work has shown that QCD axions may efficiently convert into photons in the magnetospheres of neutron stars (NSs), generating spectral lines that may be observable using near-future radio telescopes [15–27]. Axion-like particles (ALPs), arising ubiquitously in string theory from the compactification of extra dimensions [28,29] and having a comparable phenomenology to the QCD axion, represent a compelling alternative DM candidate with the potential to be observed by radio telescopes today. In this Letter we use observations of the Galactic Center (GC) from the 100-m Robert C. Byrd Green Bank Telescope (GBT), collected as part of the Breakthrough Listen (BL) project searching for extraterrestrial intelligence [30], to search for axion DM across the mass range $m_a \in (15, 35)$ μeV.

A majority of the current axion DM experiments attempt to probe the coupling of axions to electromagnetism, given by $\mathcal{L} = g_{a\gamma\gamma} a \mathbf{E} \cdot \mathbf{B}$, where $\mathbf{E}$ ($\mathbf{B}$) is the electric (magnetic) field, a is the axion field, and $g_{a\gamma\gamma}$ is a coupling constant (with units of inverse energy). In the presence of a static external magnetic field, this interaction induces a mixing between axions and electromagnetic radiation, allowing in some cases for an efficient conversion between the two. Among the most successful axion DM experiments are ADMX [31–33] and HAYSTAC [34–36], which attempt to leverage this principle using resonant cavities that are tuned to amplify electromagnetic signals generated from a particular axion mass. These experiments have set powerful constraints on the axion-photon coupling in the mass range studied here; the current limits from these experiments are illustrated in Fig. 1 (blue bands) and are shown alongside the constraints from the CAST experiment [37] (black), a recast constraint from radio observations from the GC magnetar (produced by comparing the 95% upper limit on the flux density used in [15,16,27] with Monte Carlo realizations of the GC magnetar obtained using our forward modeling framework), and the axion-photon couplings arising in the DFSZ [38,39] and KSVZ [40,41] benchmark models of the QCD axion. The two aforementioned models represent only a subset of a much broader range of QCD axions, some of which may have significantly enhanced

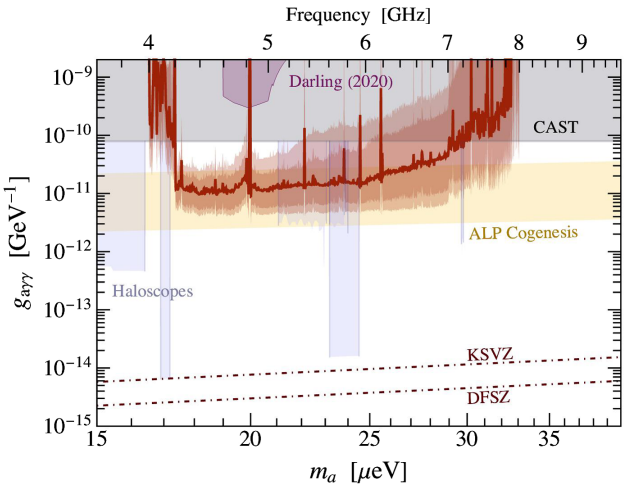

FIG. 1. Upper limit (95% confidence level) on the axion-photon coupling derived in this Letter using the BL radio observations of the GC. We illustrate the median limit over 100 MC realizations of the NS population (red line), and the corresponding 68% and 95% statistical uncertainties on the population model (see text for details). We compare our upper limit to those from the CAST [37], HAYSTAC [34,35], and ADMX [31,45] experiments, the prediction from ALP cogenesis [44], and radio observations of the GC magnetar [15,16], which we recast using our modeling (see text).

axion-photon couplings [42,43]. We also highlight in Fig. 1 the region of parameter space for which ALP DM may explain the primordial baryon asymmetry [44]—this region is labeled "ALP Cogenesis."

Despite their astronomical distances from Earth, NSs provide competitive environments in which to search for signatures of axion DM because these objects contain enormous magnetic fields (approaching, or even exceeding, field strengths of $\sim 10^{15}$ G) and are surrounded by a dilute, radially decreasing plasma [46]. Collectively these features induce strong resonant transitions between axions and photons, a process that is triggered when the plasma mass induced by the ambient charge density matches the axion rest mass [17–19,21,24,26,47].

The axion-photon conversion process in realistic NS magnetospheres (including photon refraction, photon absorption, plasma broadening, the anisotropic response of the medium, general relativistic effects, etc.) has been described and simulated with increasing complexity in recent years [20,22,24–26]. The signal appears as a narrow radio line at the frequency corresponding to the axion mass. Here, we search for the collective set of radio lines induced from the conversion of axions in the population of NSs located near the GC. Since each radio line will be Doppler shifted by the relative motion of the associated NS, the signal appears as a forest of narrow lines centered at the frequency $f = m_a/2\pi$ [20].

The GC NS population signal as observed by GBT was previously modelled in [20] using the NS population models of [48,49], which have been constructed so as to reproduce observed pulsar distributions [50]. We improve upon the population models in this Letter by incorporating more recent developments in the understanding of NS magnetic field evolution and by more carefully modeling the spatial distribution of NSs in the GC region using the observed star formation history. A search for axions from the GC NS population was previously performed using the Effelsberg 100-m telescope [23] in the L band [$m_a \in (5.2, 6.0)$ μeV] and S band [$m_a \in (9.8, 11.0)$ μeV]; relative to [23], our present search covers a broader mass range [$m_a \in (15, 35)$ μeV], makes use of more exposure time (∼280 min as opposed to ∼80 min in [23]), uses improved NS population models, and incorporates state-of-the-art simulations for the axion-photon conversion process at the level of the individual NS [24]. Observations from the Very Large Array (VLA) of the GC magnetar SGR J1745-2900 have also been interpreted in the context of axion-photon conversion [15,16,27]—a search first suggested in [19]. Our present search includes the GC magnetar within the field of view and has a stronger radio flux sensitivity, thus offering a notable improvement over the VLA analysis in the mass range studied.

Data selection and reduction.—We use C band data collected by the BL GBT GC survey [30] over four different observing dates that sampled the region of the GC using a hexagonal tiling, with a central pointing (A region, pointing denoted as `A00`), as well as an interior ring (B region) with six pointings, and an exterior ring (C region) with twelve pointings. The A region is centered at the GC, while the B region (C region) pointings are centered ∼1.8′ (∼3.6′) away from the GC. The full width at half maximum (FWHM) of the GBT beam at the central frequency of the C band is approximately 2.5′. In our analysis we use the A pointings for our signal analysis and the C pointings for vetoing putative signal candidates. We also use measurements of well-characterized flux density calibrators and strong pulsars performed during the observations as control measurements that allow us to identify and veto spurious excesses. A summary of all measurements used in this Letter is provided in Supplemental Material (SM) Table S1 [51]; note that we use the data collected on modified Julian date 58733 (30 min `A00` pointing time) and 58737 (250 min `A00` pointing time) for our signal analyses, while the data collected on the other two days are used for radio frequency interference (RFI) vetoes.

Our search attempts to identify quasimonochromatic lines ($\delta f/f \lesssim 10^{-5}$), motivating the use of the medium resolution BL data product [30], which provides a native frequency resolution of $\delta f_{\rm nat} \approx 2.8$ kHz. The data collection was performed with the dedicated dual polarization, wideband receiver at the GBT for the BL project [30,95] and spans 3.5 to 8.2 GHz. However, we consider only the 4–8 GHz range, beyond which the data quality is notably degraded. The data are characterized by regular structures

at 3 MHz intervals, which we call coarse channels, induced by the BL polyphase filter bank. There is an exponential loss in the gain at the coarse channel edges and a single-bin dc spike, which renders the central frequency channel unsuitable for inclusion in our analysis [96]. (See Ref. [97] for a related analysis.)

For each observing date, the power spectral density data for each target are recorded in 1.07 s intervals; we further filter these time intervals for time-varying RFI through a procedure described in SM [51]. Next, we mask out the dc bin and perform a 32-fold down-binning such that the coarse channel spectra are resolved by 32 sub-bins, which we refer to as the fine bins, at $\delta f \approx 91.6$ kHz width. This provides a relative frequency resolution $\delta f/f > 10^{-5}$ over the full frequency range that matches the width of the expected signal. We do not combine data across different observing dates; these are combined later through a joint likelihood. We also perform seven shifted downbinnings in order to search for signals that may be misaligned with our fiducial binning.

Analysis.—We analyze the uncalibrated `A00` data in a given coarse channel for spectral excesses that appear within a single fine bin using a combination of parametric and Gaussian process (GP) modeling. Our parametric model that describes the exponential cutoff of the data at the coarse bin edges has four model parameters (see SM [51] for the explicit form). The covariance matrix $\mathbf{K}$ for our GP model is the sum of an exponential-squared kernel, with two hyperparameters for the normalization and the correlation scale, and an exponential sine squared kernel, with three hyperparameters describing the normalization, correlation length, and oscillation period. The exponential sine squared kernel is motivated by the clear, periodic structure that is instrumental in nature and observed in every coarse channel. The exponential kernel accounts for additional instrumental and astrophysical background variations. We also include an additional hyperparameter rescaling the diagonal contribution of the statistical error to address instances in which our error estimation may not be robust. A fit of the background model to the data in an example coarse channel is illustrated in Fig. 2.

We follow the statistical approach for searching for narrow spectral excesses with hybrid GP and parametric models developed in [98,99]. In particular, we construct a likelihood ratio Λ between the model with and without a signal component, which is simply a spectral line confined to a single fine channel. We use the marginal likelihood from the GP analysis in the construction of the likelihood ratio [98]. In searching for a single fine-channel excess, we perform the fit to the combined signal and background model over the full coarse channel that contains the fine channel of interest. The discovery significance is quantified by the test statistic (TS) $t = -2\ln\Lambda$. Last, the 95% upper limits on the signal strength are determined from the profile likelihood evaluated as a function of the signal amplitude.

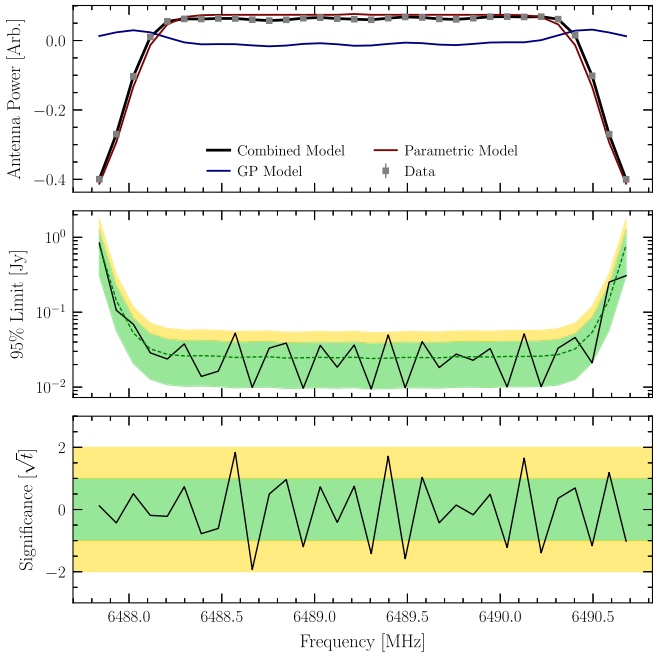

FIG. 2. Top: an illustration of the data and the fitted components of our model for a single coarse channel. Middle: the 95% CL upper limits on a flux density excess with bandwidth $\delta f = 91.6$ kHz. Bottom: the corresponding significances of the flux density excesses and deficits.

An example of the analysis as applied to a single coarse channel is depicted in Fig. 2. In the middle panel we show the 95% upper limit on the fine-channel lines while the bottom panel illustrates the detection significance, multiplied by the sign of the best-fit line amplitude. For consistency we allow the best-fit line amplitude to be both positive and negative. We power constrain the upper limit [100], which means that we do not allow the 95% upper limit to be stronger than the lower 1σ expected limit under the null hypothesis. We derive the $1/2\sigma$ expected upper limits, illustrated in Fig. 2 in green and gold, respectively, through the Asimov procedure [101].

We calibrate the data following the procedure in [102] (see SM [51]). We then join the calibrated results of the two observing sessions using a joint likelihood to obtain flux density limits and detection significances. Our flux density limits are presented in Fig. 3 versus the optimal sensitivity expected from the radiometer equation.

In the process of joining the results, we make use of the auxiliary data collected during the observing sessions to veto signal candidates coincident with RFI or astrophysical lines. We then implement a spurious signal nuisance parameter, similar to that in [99,103], to account for mismodeling and instrumental effects by incorporating information about the distribution of TSs of nearby test masses when assigning the TS to a mass point of interest. The nuisance parameter is degenerate with the signal parameter, but for a Gaussian prior with a variance determined by the distribution of nearby TS

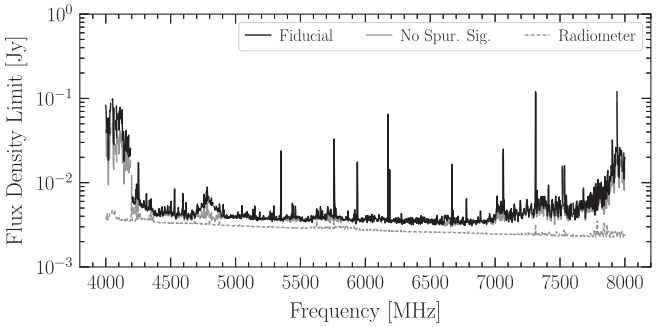

FIG. 3. A comparison of the derived flux density sensitivities (with and without the inclusion of the spurious signal nuisance parameter correction) compared with the radiometer equation expected sensitivity. For presentation, the limits have been smoothed with a median filter.

values (see SM [51] for details). The effect of the spurious signal nuisance parameter is illustrated in Fig. 3, with the curve labeled "No Spur. Sig." being the stronger limit obtained without the spurious signal analysis. In total, there remain 17 excesses at $t > 25$ including the results of both our fiducial binning and our seven additional shifted binning analyses. Three excesses appear within the expected frequency range of formaldehyde (4813.6–4834.5 MHz) and methanol (6661.8–6675.2 MHz) masers [104], while several others may be vetoed as transients or RFI after further scrutiny. Eleven excesses remain at $t > 25$ as signal candidates, but none exceed our predetermined discovery threshold of $t = 100$ (see SM [51] for details).

Results and discussion.—The expected flux density at a given frequency generated from axion conversion near a NS depends on $g_{a\gamma\gamma}$, the NS dipole magnetic field strength, the NS rotational period, the misalignment angle of the dipole axis with respect to the axis of rotation, the relative orientation of the NS with respect to Earth, the DM density near the NS, the NS velocity with respect to the Galactic frame, the DM velocity dispersion near the NS, and the NS mass and radius (which we fix to to be 1 $M_\odot$ and 10 km, respectively, as these parameters have a minimal impact on the signal). We assume that the recent NS birth rate $\Psi_{\rm NS}$ as a function of distance r from the GC is

$$\Psi_{\rm NS} = 9.4 \times 10^{-6} \left(\frac{r}{1\ \rm pc}\right)^{-1.93} \exp\left[-\frac{r}{0.5\ \rm pc}\right]\ \rm pc^{-3}\,yr^{-1}. \tag{1}$$

We generate NSs from this distribution over the past 30 Myr, though the dominant NSs for our signal typically have ages $\lesssim$1 Myr. The exponential cutoff at $\sim$0.5 pc encodes the fact that there is no active star formation (though there is potentially protostar formation) within the circumnuclear ring from 1 to 3 pc [105]. The slope of the density profile near the GC is set to match that observed for young stars [106]. The normalization in (1) is set by a combination of the recent star formation rate in the inner pc, estimated as $\sim 4 \times 10^{-3}\ M_\odot\,\rm yr^{-1}$ with a top-heavy initial mass function of $dN/dM \propto M^{-1.7}$ observed in the inner pc [107], for stellar mass M, calculated over the range 1–150 $M_\odot$, and the assumption that stars born with initial masses between 8 $M_\odot$ and 20 $M_\odot$ form NSs [108]. Intriguingly, we note that this star-formation rate predicts the existence of $\sim$0.25 magnetars in the GC [109], roughly consistent with the observation of one such object at a projected distance of $\sim$0.17 pc from the central black hole [110]. We condition our randomly generated NS population models on the existence of this magnetar; we require the existence of a NS with a magnetic field today above 5×10^{13} G and with a projected angular distance of 2.4 ± 0.6 arcsec from the GC (consistent with observations at $\pm 2\sigma$) [111].

The dipole magnetic field strength B evolves from its initial value at birth through Ohmic dissipation and Hall diffusion [20,112–114]. We evolve the NS period and misalignment angle according to the equations for coupled magneto-rotational evolution, following [115]. As in [20] the initial period distribution is taken to be normally distributed, for positive periods only, and the initial magnetic field distribution is log-normally distributed; the parameters of these distributions are taken from model 1 in [20] and model B1 in [114], which performed population synthesis studies comparing the predicted pulsar populations in these models to the Australia Telescope National Facility pulsar catalog [50]. We describe the NS magnetosphere using the charge-separated Goldreich-Julian (GJ) model [46], which is expected to be a good description of the closed-field regions of active pulsars [116,117]. We assume that the plasma frequency in the negatively charged regions of the plasma is set by the charge-separated electrons, while in the positive region it is determined by positrons (in active pulsars) and ions (in dead NSs).

We describe the DM distribution using a Navarro-Frenk-White (NFW) [118,119] profile, fixing the scale radius to 20 kpc and normalizing the distribution such that the local DM density is 0.346 $\rm GeV/cm^3$. Note that recent simulations [120–124] suggest that the DM profile may be contracted beyond the NFW profile in the inner kiloparsec because of baryonic feedback, which would further enhance our signal though a cored profile, which could eliminate our sensitivity to new parameter space, is also possible [125]), though we do not consider such a possibility here.

In order to compute the flux density from each NS in the population, we use an updated version of the ray tracer developed in [24]. For each NS, this procedure amounts to Monte Carlo (MC) sampling the axion phase space density at the axion-photon conversion surface, computing the local axion-specific conversion probability, propagating photons to the light cylinder using a highly magnetized cold plasma dispersion relation, and retroactively reweighting samples to include resonant cyclotron absorption and refraction induced

axion-photon de-phasing. Photons are plasma broadened as described in [22,24,25] and Doppler shifted according to the projected line of sight velocity of the NS (see SM [51]). We extract the observable time-averaged differential power at each frequency and apply to each NS in the population the GBT efficiency function, which accounts for the suppression in sensitivity for objects off of the beam axis.

It is crucial to work beyond leading order in the axion-photon conversion probability, which has not been done in previous radio searches (e.g., [15,16,23,27]). Those analyses naively applied the leading-order perturbative results for the conversion probabilities in the NS magnetospheres such that at their upper limit values for $g_{a\gamma\gamma}$ the conversion probabilities evaluate to well beyond unity. We address this issue by exponentiating the leading-order perturbative conversion probabilities following the Landau-Zener formalism (see, e.g., [22] and SM [51]). At large $g_{a\gamma\gamma}$ axion-photon conversion becomes adiabatic, leading to conversion probabilities $P_{a\to\gamma} \sim P_{\gamma\to a} \sim 1$; since each axion-photon trajectory invariably crosses an even number of conversion surfaces, the probability of an infalling axion state transitioning to an outgoing photon becomes exponentially suppressed.

The collective flux density from all NSs in a population is then compared with the flux density limit in Fig. 3. The ensemble of NSs from the population produce signals across multiple coarse bins, because of the relative Doppler shifts, such that the brightest single fine bin typically arises from a single NS. The 95% upper limit on $|g_{a\gamma\gamma}|$ that we determine from this Letter is shown in Fig. 1. The solid red curve denotes the 95% statistical upper limit, but the median limit over all MC realizations of the NS population (conditioned on the existence of the GC magnetar). The dark and light shaded red regions show the 68% and 95% containment intervals for the limit over the full ensemble of realizations. These curves have been smoothed for clarity; the sensitivity is only moderately degraded if the brightest NS falls near a course-bin edge because the next-brightest NS typically provides a comparable sensitivity (see SM [51] Fig. S7). Our upper limit probes unexplored axion parameter space below the existing CAST limit and constrains the ALP cogenesis scenario [44] shaded in yellow, where ALPs can explain the primordial baryon asymmetry.

A qualitative improvement in sensitivity to an axion signal may be obtained in the future with the proposed Square Kilometer Array (SKA). As we show in Supplemental Material, Fig. S8 [51], the SKA Phase 2 array [20,126], assumed to have 5600 15-m telescopes and 100 h of observing time, could achieve a 10σ discovery sensitivity for $|g_{a\gamma\gamma}| \gtrsim \text{few} \times 10^{-13}\ \text{GeV}^{-1}$. Given that QCD axion DM may naturally explain the DM abundance in this mass range, the possibility of such a result serves as motivation for continuing to construct large telescope arrays capable of deep searches of the GC region.

We thank C. Dessert, T. Edwards, A. Millar, A. Goobar, K. van Bibber, and J. McDonald for useful discussions. J. W. F was supported by a Pappalardo Fellowship. B. R. S. was supported in part by the DOE Early Career Grant No. DESC0019225. M. L. and T. L. are supported by the European Research Council under Grant No. 742104. T. L. is also partially supported by the Swedish Research Council under Contract No. 2019-05135 and the Swedish National Space Agency under Contract No. 117/19. S. J. W. and C. W. were supported by the European Research Council (ERC) under the European Union's Horizon 2020 research and innovation programme (Grant Agreement No. 864035–Un-Dark). This research used resources from the Lawrencium computational cluster provided by the IT Division at the Lawrence Berkeley National Laboratory, supported by the Director, Office of Science, and Office of Basic Energy Sciences, of the U.S. Department of Energy under Contract No. DE-AC02-05CH11231.

*jwfoster@mit.edu
†s.j.witte@uva.nl
‡brsafdi@berkeley.edu

[1] R. D. Peccei and Helen R. Quinn, *CP* Conservation in the Presence of Instantons, Phys. Rev. Lett. **38**, 1440 (1977).
[2] R. D. Peccei and Helen R. Quinn, Constraints imposed by *CP* conservation in the presence of instantons, Phys. Rev. D **16**, 1791 (1977).
[3] Steven Weinberg, A New Light Boson?, Phys. Rev. Lett. **40**, 223 (1978).
[4] Frank Wilczek, Problem of Strong *P* and *T* Invariance in the Presence of Instantons, Phys. Rev. Lett. **40**, 279 (1978).
[5] John Preskill, Mark B. Wise, and Frank Wilczek, Cosmology of the invisible axion, Phys. Lett. **120B**, 127 (1983).
[6] L. F. Abbott and P. Sikivie, A cosmological bound on the invisible axion, Phys. Lett. **120B**, 133 (1983).
[7] Michael Dine and Willy Fischler, The not so harmless axion, Phys. Lett. **120B**, 137 (1983).
[8] David J. E. Marsh, Axion cosmology, Phys. Rep. **643**, 1 (2016).
[9] Vincent B. Klaer and Guy D. Moore, The dark-matter axion mass, J. Cosmol. Astropart. Phys. 11 (2017) 049.
[10] Marco Gorghetto, Edward Hardy, and Giovanni Villadoro, Axions from strings: The attractive solution, J. High Energy Phys. 07 (2018) 151.
[11] Malte Buschmann, Joshua W. Foster, and Benjamin R. Safdi, Early-Universe Simulations of the Cosmological Axion, Phys. Rev. Lett. **124**, 161103 (2020).
[12] Marco Gorghetto, Edward Hardy, and Giovanni Villadoro, More axions from strings, SciPost Phys. **10**, 050 (2021).
[13] Michael Dine, Nicolas Fernandez, Akshay Ghalsasi, and Hiren H. Patel, Comments on axions, domain walls, and cosmic strings, J. Cosmol. Astropart. Phys. 11 (2021) 041.
[14] Malte Buschmann, Joshua W. Foster, Anson Hook, Adam Peterson, Don E. Willcox, Weiqun Zhang, and Benjamin R. Safdi, Dark matter from axion strings with adaptive mesh refinement, Nat. Commun. **13**, 1049 (2022).

[15] Jeremy Darling, New limits on axionic dark matter from the magnetar PSR J1745-2900, Astrophys. J. Lett. **900**, L28 (2020).
[16] Jeremy Darling, Search for Axionic Dark Matter Using the Magnetar PSR J1745-2900, Phys. Rev. Lett. **125**, 121103 (2020).
[17] M. S. Pshirkov, Conversion of dark matter axions to photons in magnetospheres of neutron stars, J. Exp. Theor. Phys. **108**, 384 (2009).
[18] Fa Peng Huang, Kenji Kadota, Toyokazu Sekiguchi, and Hiroyuki Tashiro, Radio telescope search for the resonant conversion of cold dark matter axions from the magnetized astrophysical sources, Phys. Rev. D **97**, 123001 (2018).
[19] Anson Hook, Yonatan Kahn, Benjamin R. Safdi, and Zhiquan Sun, Radio Signals from Axion Dark Matter Conversion in Neutron Star Magnetospheres, Phys. Rev. Lett. **121**, 241102 (2018).
[20] Benjamin R. Safdi, Zhiquan Sun, and Alexander Y. Chen, Detecting axion dark matter with radio lines from neutron star populations, Phys. Rev. D **99**, 123021 (2019).
[21] Mikaël Leroy, Marco Chianese, Thomas D. P. Edwards, and Christoph Weniger, Radio signal of axion-photon conversion in neutron stars: A ray tracing analysis, Phys. Rev. D **101**, 123003 (2020).
[22] Richard A. Battye, Bjoern Garbrecht, Jamie I. McDonald, Francesco Pace, and Sankarshana Srinivasan, Dark matter axion detection in the radio/mm-waveband, Phys. Rev. D **102**, 023504 (2020).
[23] Joshua W. Foster, Yonatan Kahn, Oscar Macias, Zhiquan Sun, Ralph P. Eatough, Vladislav I. Kondratiev, Wendy M. Peters, Christoph Weniger, and Benjamin R. Safdi, Green Bank and Effelsberg Radio Telescope Searches for Axion Dark Matter Conversion in Neutron Star Magnetospheres, Phys. Rev. Lett. **125**, 171301 (2020).
[24] Samuel J. Witte, Dion Noordhuis, Thomas D. P. Edwards, and Christoph Weniger, Axion-photon conversion in neutron star magnetospheres: The role of the plasma in the Goldreich-Julian model, Phys. Rev. D **104**, 103030 (2021).
[25] R. A. Battye, B. Garbrecht, J. I. McDonald, and S. Srinivasan, Radio line properties of axion dark matter conversion in neutron stars, J. High Energy Phys. 09 (2021) 105.
[26] Alexander J. Millar, Sebastian Baum, Matthew Lawson, and M. C. David Marsh, Axion-photon conversion in strongly magnetised plasmas, J. Cosmol. Astropart. Phys. 11 (2021) 013.
[27] R. A. Battye, J. Darling, J. McDonald, and S. Srinivasan, Towards robust constraints on axion dark matter using PSR J1745-2900, Phys. Rev. D **105**, L021305 (2022).
[28] Peter Svrcek and Edward Witten, Axions in string theory, J. High Energy Phys. 06 (2006) 051.
[29] Asimina Arvanitaki, Savas Dimopoulos, Sergei Dubovsky, Nemanja Kaloper, and John March-Russell, String axiverse, Phys. Rev. D **81**, 123530 (2010).
[30] Vishal Gajjar *et al.*, The breakthrough listen search for intelligent life near the Galactic Center. I., Astron. J. **162**, 33 (2021).
[31] T. Braine *et al.* (ADMX Collaboration), Extended Search for the Invisible Axion with the Axion Dark Matter Experiment, Phys. Rev. Lett. **124**, 101303 (2020).
[32] N. Du *et al.* (ADMX Collaboration), A Search for Invisible Axion Dark Matter with the Axion Dark Matter Experiment, Phys. Rev. Lett. **120**, 151301 (2018).
[33] Nathan Woollett and Gianpaolo Carosi, Photonic band gap cavities for a future ADMX, Springer Proc. Phys. **211**, 61 (2018).
[34] L. Zhong *et al.* (HAYSTAC Collaboration), Results from phase 1 of the HAYSTAC microwave cavity axion experiment, Phys. Rev. D **97**, 092001 (2018).
[35] K. M. Backes *et al.* (HAYSTAC Collaboration), A quantum-enhanced search for dark matter axions, Nature (London) **590**, 238 (2021).
[36] K. M. Backes *et al.* (HAYSTAC Collaboration), A quantum-enhanced search for dark matter axions, Nature (London) **590**, 238 (2021).
[37] V. Anastassopoulos *et al.* (CAST Collaboration), New CAST limit on the axion-photon interaction, Nat. Phys. **13**, 584 (2017).
[38] Michael Dine, Willy Fischler, and Mark Srednicki, A simple solution to the strong *CP* problem with a harmless axion, Phys. Lett. **104B**, 199 (1981).
[39] A. R. Zhitnitsky, On possible suppression of the axion hadron interactions, Yad. Fiz. **31**, 497 (1980) [Sov. J. Nucl. Phys. **31**, 260 (1980)].
[40] Jihn E. Kim, Weak Interaction Singlet and Strong *CP* Invariance, Phys. Rev. Lett. **43**, 103 (1979).
[41] Mikhail A. Shifman, A. I. Vainshtein, and Valentin I. Zakharov, Can confinement ensure natural *CP* invariance of strong interactions?, Nucl. Phys. **B166**, 493 (1980).
[42] Marco Farina, Duccio Pappadopulo, Fabrizio Rompineve, and Andrea Tesi, The photo-philic QCD axion, J. High Energy Phys. 01 (2017) 095.
[43] Anton V. Sokolov and Andreas Ringwald, Photophilic hadronic axion from heavy magnetic monopoles, J. High Energy Phys. 06 (2021) 123.
[44] Raymond T. Co, Lawrence J. Hall, and Keisuke Harigaya, Predictions for axion couplings from ALP cogenesis, J. High Energy Phys. 01 (2021) 172.
[45] C. Bartram *et al.* (ADMX Collaboration), Search for Invisible Axion Dark Matter in the 3.3–4.2 μeV Mass Range, Phys. Rev. Lett. **127**, 261803 (2021).
[46] P. Goldreich and W. H. Julian, Pulsar electrodynamics, Astrophys. J. **157**, 869 (1969).
[47] Georg Raffelt and Leo Stodolsky, Mixing of the photon with low mass particles, Phys. Rev. D **37**, 1237 (1988).
[48] Claude-Andre Faucher-Giguere and Victoria M. Kaspi, Birth and evolution of isolated radio pulsars, Astrophys. J. **643**, 332 (2006).
[49] S. B. Popov, J. A. Pons, J. A. Miralles, P. A. Boldin, and B. Posselt, Population synthesis studies of isolated neutron stars with magnetic field decay, Mon. Not. R. Astron. Soc. **401**, 2675 (2010).
[50] R. N. Manchester, G. B. Hobbs, A. Teoh, and M. Hobbs, The Australia Telescope National Facility pulsar catalogue, Astron. J. **129**, 1993 (2005).
[51] See Supplemental Material at http://link.aps.org/supplemental/10.1103/PhysRevLett.129.251102 for further details on data selection, reduction, calibration and analysis, and fully characterize the neutron star population modeling and the procedure for predicting axion conversion signals

form neutron stars at the galactic center. Systematic tests and variations of the analysis and forward modeling procedure are also included, which includes Refs. [52–94].
[52] Emily Ramey, Nick Joslyn, Richard Prestage, Mark Whitehead, Michael Timothy Lam, Tim Blattner, Luke Hawkins, Cedric Viou, and Jessica Masson, Real-time RFI mitigation in pulsar observations, in *American Astronomical Society Meeting Abstracts #231, American Astronomical Society Meeting Abstracts* (2018), Vol. 231, p. 150.06.
[53] C. J. Law, F. Yusef-Zadeh, W. D. Cotton, and R. J. Maddalena, GBT multiwavelength survey of the Galactic Center region, Astrophys. J. Suppl. Ser. **177**, 255 (2008).
[54] Kaustubh Rajwade, Duncan Lorimer, and Loren Anderson, Detecting pulsars in the Galactic Centre, Mon. Not. R. Astron. Soc. **471**, 730 (2017).
[55] GBT Support Staff, Proposer's guide for the green bank telescope, https://science.nrao.edu/facilities/gbt/proposing/GBTpg.pdf (2017).
[56] Vishal Gajjar (personal communication).
[57] D. Bhattacharya, Evolution of neutron star magnetic fields, J. Astrophys. Astron. **23**, 67 (2002).
[58] Andrew Cumming, Phil Arras, and Ellen G. Zweibel, Magnetic field evolution in neutron star crusts due to the Hall effect and Ohmic decay, Astrophys. J. **609**, 999 (2004).
[59] K. N. Gourgouliatos and A. Cumming, Hall effect in neutron star crusts: evolution, endpoint and dependence on initial conditions, Mon. Not. R. Astron. Soc. **438**, 1618 (2014).
[60] A. Generozov, N. C. Stone, B. D. Metzger, and J. P. Ostriker, An overabundance of black hole x-ray binaries in the Galactic Centre from tidal captures, Mon. Not. R. Astron. Soc. **478**, 4030 (2018).
[61] S. D. Tremaine, J. P. Ostriker, and L. Spitzer, Jr., The formation of the nuclei of galaxies. I. M31., Astrophys. J. **196**, 407 (1975).
[62] Oleg Y. Gnedin, Jeremiah P. Ostriker, and Scott Tremaine, Co-evolution of galactic nuclei and globular cluster systems, Astrophys. J. **785**, 71 (2014).
[63] Marc Freitag, Pau Amaro-Seoane, and Vassiliki Kalogera, Stellar remnants in Galactic nuclei: Mass segregation, Astrophys. J. **649**, 91 (2006).
[64] Rebecca K. Leane, Tim Linden, Payel Mukhopadhyay, and Natalia Toro, Celestial-body focused dark matter annihilation throughout the Galaxy, Phys. Rev. D **103**, 075030 (2021).
[65] J. M. Cordes and T. Joseph W. Lazio, Anomalous radio-wave scattering from interstellar plasma structures, Astrophys. J. **549**, 997 (2001).
[66] Geoffrey C. Bower, W. M. Goss, Heino Falcke, Donald C. Backer, and Yoram Lithwick, The intrinsic size of sagittarius A* from 0.35 to 6 cm, Astrophys. J. Lett. **648**, L127 (2006).
[67] A. T. Barnes, S. N. Longmore, C. Battersby, J. Bally, J. M. D. Kruijssen, J. D. Henshaw, and D. L. Walker, Star formation rates and efficiencies in the Galactic Centre, Mon. Not. R. Astron. Soc. **469**, 2263 (2017).
[68] F. Yusef-Zadeh, J. H. Lacy, M. Wardle, B. Whitney, H. Bushouse, D. A. Roberts, and R. G. Arendt, Massive star formation of the Sgr A East H II regions near the Galactic Center, Astrophys. J. **725**, 1429 (2010).
[69] H. Bartko *et al.*, An extremely top-heavy initial mass function in the Galactic Center stellar disks, Astrophys. J. **708**, 834 (2010).
[70] F. Yusef-Zadeh, M. Wardle, D. Kunneriath, M. Royster, A. Wootten, and D. A. Roberts, ALMA detection of bipolar outflows: Evidence for low-mass star formation within 1 pc of Sgr A*, Astrophys. J. Lett. **850**, L30 (2017).
[71] Paul T. P. Ho, Luis C. Ho, John C. Szczepanski, James M. Jackson, and J. Thomas Armstrong, A molecular gas streamer feeding the Galactic Centre, Nature (London) **350**, 309 (1991).
[72] Masato Tsuboi, Yoshimi Kitamura, Kenta Uehara, Takahiro Tsutsumi, Ryosuke Miyawaki, Makoto Miyoshi, and Atsushi Miyazaki, ALMA view of the circumnuclear disk of the Galactic Center: Tidally disrupted molecular clouds falling to the Galactic Center, Publ. Astron. Soc. Jpn. **70**, 85 (2018).
[73] O. Pfuhl, T. K. Fritz, M. Zilka, H. Maness, F. Eisenhauer, R. Genzel, S. Gillessen, T. Ott, K. Dodds-Eden, and A. Sternberg, The star formation history of the Milky Way's nuclear star cluster, Astrophys. J. **741**, 108 (2011).
[74] Mark R. Krumholz, J. M. Diederik Kruijssen, and Roland M. Crocker, A dynamical model for gas flows, star formation and nuclear winds in Galactic Centres, Mon. Not. R. Astron. Soc. **466**, 1213 (2017).
[75] Mark R. Krumholz and J. M. Diederik Kruijssen, A dynamical model for the formation of gas rings and episodic starbursts near Galactic Centres, Mon. Not. R. Astron. Soc. **453**, 739 (2015).
[76] S. Gillessen, F. Eisenhauer, S. Trippe, T. Alexander, R. Genzel, F. Martins, and T. Ott, Monitoring stellar orbits around the Massive Black Hole in the Galactic Center, Astrophys. J. **692**, 1075 (2009).
[77] Peter Goldreich and Andreas Reisenegger, Magnetic field decay in isolated neutron stars, Astrophys. J. **395**, 250 (1992).
[78] José A Pons, Daniele Viganò, and Nanda Rea, A highly resistive layer within the crust of x-ray pulsars limits their spin periods, Nat. Phys. **9**, 431 (2013).
[79] Daniele Viganò, Nanda Rea, Jose A. Pons, Rosalba Perna, Deborah N. Aguilera, and Juan A. Miralles, Unifying the observational diversity of isolated neutron stars via magneto-thermal evolution models, Mon. Not. R. Astron. Soc. **434**, 123 (2013).
[80] Andrea Passamonti, Taner Akgün, José A. Pons, and Juan A. Miralles, The relevance of ambipolar diffusion for neutron star evolution, Mon. Not. R. Astron. Soc. **465**, 3416 (2016).
[81] Jose A. Pons and U. Geppert, Magnetic field dissipation in neutron star crusts: From magnetars to isolated neutron stars, Astron. Astrophys. **470**, 303 (2007).
[82] P. B. Jones, Heterogeneity of solid neutron-star matter: Transport coefficients and neutrino emissivity, Mon. Not. R. Astron. Soc. **351**, 956 (2004).
[83] P. B. Jones, Disorder Resistivity of Solid Neutron-Star Matter, Phys. Rev. Lett. **93**, 221101 (2004).
[84] Elliott Flowers and Malvin A. Ruderman, Evolution of pulsar magnetic fields, Astrophys. J. **215**, 302 (1977).

[85] P. B. Jones, First-principles point-defect calculations for solid neutron star matter, Mon. Not. R. Astron. Soc. **321**, 167 (2001).

[86] Simon Johnston and Aris Karastergiou, Pulsar braking and the P-$\dot{P}$ diagram, Mon. Not. R. Astron. Soc. **467**, 3493 (2017).

[87] Moqbil S. Alenazi and Paolo Gondolo, Phase-space distribution of unbound dark matter near the Sun, Phys. Rev. D **74**, 083518 (2006).

[88] Samoil M. Bilenky and S. T. Petcov, Massive neutrinos and neutrino oscillations, Rev. Mod. Phys. **59**, 671 (1987); **61**, 169(E) (1989); **60**, 575(E) (1988).

[89] Philip F. Hopkins *et al.*, FIRE-2 simulations: Physics versus numerics in galaxy formation, Mon. Not. R. Astron. Soc. **480**, 800 (2018).

[90] Daniel McKeown, James S. Bullock, Francisco J. Mercado, Zachary Hafen, Michael Boylan-Kolchin, Andrew Wetzel, Lina Necib, Philip F. Hopkins, and Sijie Yu, Amplified J-factors in the Galactic Centre for velocity-dependent dark matter annihilation in FIRE simulations, Mon. Not. R. Astron. Soc. **513**, 55 (2022).

[91] Luca Di Luzio, Federico Mescia, and Enrico Nardi, Redefining the Axion Window, Phys. Rev. Lett. **118**, 031801 (2017).

[92] Kaya Mori, Eric V. Gotthelf, Shuo Zhang, Hongjun An, Frederick K. Baganoff, Nicolas M. Barriere, Andrei M. Beloborodov, Steven E. Boggs, Finn E. Christensen, William W. Craig *et al.*, Nustar discovery of a 3.76 s transient magnetar near Sagittarius A, Astrophys. J. Lett. **770**, L23 (2013).

[93] Andrei P. Igoshev, Rainer Hollerbach, Toby Wood, and Konstantinos N. Gourgouliatos, Strong toroidal magnetic fields required by quiescent x-ray emission of magnetars, Nat. Astron. **5**, 145 (2021).

[94] J. A. Kennea, D. N. Burrows, C. Kouveliotou, D. M. Palmer, Ersin Göğüş, Yuki Kaneko, P. A. Evans, N. Degenaar, M. T. Reynolds, J. M. Miller *et al.*, Swift discovery of a new soft gamma repeater, SGR J1745–29, near Aagittarius A, Astrophys. J. Lett. **770**, L24 (2013).

[95] David H. E. MacMahon *et al.*, The breakthrough listen search for intelligent life: A wideband data recorder system for the Robert C. Byrd green bank telescope, Publ. Astron. Soc. Pac. **130**, 044502 (2018).

[96] Matthew Lebofsky *et al.*, The breakthrough listen search for intelligent life: Public data, formats, reduction, and archiving, Publ. Astron. Soc. Pac. **131**, 124505 (2019).

[97] Aya Keller, Sean O'Brien, Adyant Kamdar, Nicholas Rapidis, Alexander Leder, and Karl van Bibber, A model-independent radio telescope dark matter search, Astrophys. J. **927**, 71 (2022).

[98] Meghan Frate, Kyle Cranmer, Saarik Kalia, Alexander Vandenberg-Rodes, and Daniel Whiteson, Modeling smooth backgrounds and generic localized signals with Gaussian processes, arXiv:1709.05681.

[99] Joshua W. Foster, Marius Kongsore, Christopher Dessert, Yujin Park, Nicholas L. Rodd, Kyle Cranmer, and Benjamin R. Safdi, Deep Search for Decaying Dark Matter with XMM-Newton Blank-Sky Observations, Phys. Rev. Lett. **127**, 051101 (2021).

[100] Glen Cowan, Kyle Cranmer, Eilam Gross, and Ofer Vitells, Power-constrained limits, arXiv:1105.3166.

[101] Glen Cowan, Kyle Cranmer, Eilam Gross, and Ofer Vitells, Asymptotic formulae for likelihood-based tests of new physics, Eur. Phys. J. C **71**, 1554 (2011); **73**, 2501(E) (2013);

[102] Akshay Suresh, James M. Cordes, Shami Chatterjee, Vishal Gajjar, Karen I. Perez, Andrew P. V. Siemion, and Danny C. Price, 4–8 GHz spectro-temporal emission from the Galactic Center magnetar PSR J1745-2900, Astrophys. J. **921**, 101 (2021).

[103] Georges Aad *et al.* (ATLAS Collaboration), Measurement of Higgs boson production in the diphoton decay channel in pp collisions at center-of-mass energies of 7 and 8 TeV with the ATLAS detector, Phys. Rev. D **90**, 112015 (2014).

[104] IAU list of important spectral lines, https://www.craf.eu/iau-list-of-important-spectral-lines.

[105] F. Yusef-Zadeh, J. Braatz, M. Wardle, and D. Roberts, Massive star formation in the molecular ring orbiting the black hole at the Galactic Center, Astrophys. J. **683**, L147 (2008).

[106] T. Do, J. R. Lu, A. M. Ghez, M. R. Morris, S. Yelda, G. D. Martinez, S. A. Wright, and K. Matthews, Stellar populations in the central 0.5 pc of the galaxy. I. A new method for constructing luminosity functions and surface-density profiles, Astrophys. J. **764**, 154 (2013).

[107] J. R. Lu, T. Do, A. M. Ghez, M. R. Morris, S. Yelda, and K. Matthews, Stellar populations in the central 0.5 pc of the galaxy. II. The initial mass function, Astrophys. J. **764**, 155 (2013).

[108] Chris L. Fryer, Mass limits for black hole formation, Astrophys. J. **522**, 413 (1999).

[109] Paz Beniamini, Kenta Hotokezaka, Alexander van der Horst, and Chryssa Kouveliotou, Formation rates and evolution histories of magnetars, Mon. Not. R. Astron. Soc. **487**, 1426 (2019).

[110] Kaya Mori *et al.*, NuSTAR discovery of a 3.76 s transient magnetar near Sagittarius A*, Astrophys. J. Lett. **770**, L23 (2013).

[111] Nanda Rea, Paolo Esposito, José A Pons, Roberto Turolla, Diego F Torres, Gian Luca Israel, Andrea Possenti, Marta Burgay, Daniele Viganò, Alessandro Papitto *et al.*, A strongly magnetized pulsar within the grasp of the Milky Way's supermassive black hole, Astrophys. J. Lett. **775**, L34 (2013).

[112] Deborah N. Aguilera, Jose A. Pons, and Juan A. Miralles, The impact of magnetic field on the thermal evolution of neutron stars, Astrophys. J. Lett. **673**, L167 (2008).

[113] S. B. Popov, J. A. Pons, J. A. Miralles, P. A. Boldin, and B. Posselt, Population synthesis studies of isolated neutron stars with magnetic field decay, Mon. Not. R. Astron. Soc. **401**, 2675 (2010).

[114] Miguel Gullón, Juan A. Miralles, Daniele Viganò, and José A. Pons, Population synthesis of isolated neutron stars with magneto-rotational evolution, Mon. Not. R. Astron. Soc. **443**, 1891 (2014).

[115] Alexander Philippov, Alexander Tchekhovskoy, and Jason G. Li, Time evolution of pulsar obliquity angle from 3D simulations of magnetospheres, Mon. Not. R. Astron. Soc. **441**, 1879 (2014).

[116] Alexander A. Philippov, Anatoly Spitkovsky, and Benoit Cerutti, Ab-initio pulsar magnetosphere: Three-dimensional particle-in-cell simulations of oblique pulsars, Astrophys. J. Lett. **801**, L19 (2015).

[117] Rui Hu and Andrei M. Beloborodov, Axisymmetric pulsar magnetosphere revisited, arXiv:2109.03935.

[118] Julio F. Navarro, Carlos S. Frenk, and Simon D. M. White, The structure of cold dark matter halos, Astrophys. J. **462**, 563 (1996).

[119] Julio F. Navarro, Carlos S. Frenk, and Simon D. M. White, A universal density profile from hierarchical clustering, Astrophys. J. **490**, 493 (1997).

[120] Joop Schaye *et al.*, The EAGLE project: Simulating the evolution and assembly of galaxies and their environments, Mon. Not. R. Astron. Soc. **446**, 521 (2015).

[121] Robert J. J. Grand, Facundo A. Gómez, Federico Marinacci, Ruediger Pakmor, Volker Springel, David J. R. Campbell, Carlos S. Frenk, Adrian Jenkins, and Simon D. M. White, The Auriga project: The properties and formation mechanisms of disc galaxies across cosmic time, Mon. Not. R. Astron. Soc. **467**, 179 (2017).

[122] Azadeh Fattahi, Julio F. Navarro, Till Sawala, Carlos S. Frenk, Kyle A. Oman, Robert A. Crain, Michelle Furlong, Matthieu Schaller, Joop Schaye, Tom Theuns, and Adrian Jenkins, The APOSTLE project: Local Group kinematic mass constraints and simulation candidate selection, Mon. Not. R. Astron. Soc. **457**, 844 (2016).

[123] Till Sawala, Carlos S. Frenk, Azadeh Fattahi, Julio F. Navarro, Richard G. Bower, Robert A. Crain, Claudio Dalla Vecchia, Michelle Furlong, John. C. Helly, Adrian Jenkins, Kyle A. Oman, Matthieu Schaller, Joop Schaye, Tom Theuns, James Trayford, and Simon D. M. White, The APOSTLE simulations: Solutions to the Local Group's cosmic puzzles, Mon. Not. R. Astron. Soc. **457**, 1931 (2016).

[124] Marius Cautun, Alejandro Benítez-Llambay, Alis J. Deason, Carlos S. Frenk, Azadeh Fattahi, Facundo A. Gómez, Robert J. J. Grand, Kyle A. Oman, Julio F. Navarro, and Christine M. Simpson, The Milky Way total mass profile as inferred from Gaia DR2, Mon. Not. R. Astron. Soc. **494**, 4291 (2020).

[125] James S. Bullock and Michael Boylan-Kolchin, Small-scale challenges to the ΛCDM paradigm, Annu. Rev. Astron. Astrophys. **55**, 343 (2017).

[126] SKA Whitepaper, https://www.skatelescope.org/wp-content/uploads/2014/03/SKA-TEL-SKO-0000308_SKA1_System_Baseline_v2_DescriptionRev01-part-1-signed.pdf (accessed: 2022-01-31).